Real-Time Hardware Emulation of a Power Take-off Model for Grid-connected Tidal Energy Systems

Nuh Erdogan[1], Donal B. Murray[1], Jochen Giebhardt[2] , Matthias Wecker[2], James Donegan[3]

[1]*Marine and Renewable Energy Centre, University College Cork,* Cork, Ireland.
{*nuh.erdogan*,*donalbmurray*}@ucc.ie
[2]*Fraunhofer Institute for Energy Economics and Energy System Technology,* Germany.
{*jochen.giebhardt*,*matthias.wecker*}@iee.fraunhofer.de
[3]*Ocean Renewable Power Company, LLC,* Dublin, Ireland.
jdonegan@orpc.co

***Abstract*—This paper describes the dynamic models of the complete power take-off system (PTO) for grid-connected tidal energy systems and performs its real-time simulation on a parallel hardware platform. It is aimed at *(i)* validating the system concept by showing if the operational performance and limits of the PTO meet the requirements set by the turbine, *(ii)* providing the real-time simulation as a development tool for the control algorithms. It is shown that the presented level of modeling and real-time analysis are a good foundation for a performance assessment of the overall system control prior to any installation of the hydro-kinetic turbine.**

***Index Terms*—electric drive, hardware-in-the-loop, hydro-kinetic turbine, PMSM, real-time simulation, tidal energy.**

I. Introduction

Tidal energy systems (TESs) have been demonstrated in many installed plants worldwide [1]. The related ocean renewable energy sector has utilized technology from the wind energy and marine sectors and incorporated it directly into the applied design [2]. This approach often results in shortcomings in performance, reliability, and survivability, as interactions between power take-off systems (PTOs) and marine components are not fully addressed or captured in the design process. To help economic viability, lowering the high levelized cost of electricity (LCOE) by improving operational reliability and resilience of TESs has therefore been a recent primary research focus [3], [4].

The prime mover considered is a horizontal axis hydro-kinetic cross-flow turbine with three foils. Cross-flow turbines typically produce a torque pulse for each of the foils in the turbine over one rotation. Even though a relatively uniform torque output is obtained when the output torque of all foils on the turbine are summed over a full rotation, torque ripples still exist. In controlling the power output of the generator coupled to the turbine, due to the large inertia of the turbine, the control time constant is too large to account for the torque transients [5]. This resulted in poor power quality being delivered to the grid. Therefore, delivering a viable PTO designed specifically for TESs requires the development and testing validation of optimal control strategies. This task aims at not only maximizing the power and energy output of the prime mover, but also increasing power quality, reducing down-time and improving system robustness.

Offline simulation has been the major tool used in developing control strategies for the grid integration of electric drive systems [6], [7]. However, this task is computationally prohibitive with offline simulation tools that unables to connect the developed controller hardware in the loop [8], [9]. The need to simulate PTO systems in real-time and test them in a non-risky environment gave rise to the concept of real-time simulation on parallel hardware platforms [10], [11]. Parallel hardware platforms are becoming convenient means for testing and validating developed controllers in different architecture configurations like hardware-in-the-loop (HIL) before prototyping [12]. In a real-time simulation, model variables of the system are produced and alter accurately within the same length of time as real world time. Hence, a real-time emulated PTO model can allow one to evaluate the impact of developed control strategies under a wide range of situations and extreme conditions in a non-destructive environment before the field implementation. Furthermore, it would make it possible to test the developed PTO controller hardware on the grid under HIL architecture.

The aim of this study is to present a real-time simulation as a development tool in designing the PTO controller for a grid-connected TES, which will be used later on in the actual system laboratory testing. The complete PTO modelis developed in MATLAB®/Simulink®, and emulated in real-time on a multi-core CPU and FPGA-based hybrid hardware platform. The characteristic of the turbine for a given water flow condition is simulated and used as input to the real-time simulation. The impact of the PTO controller on the grid is evaluated through the real-time analysis. Real-time simulation results are presented to explore system limits and show the impact of the developed PTO on the grid. To evaluate the impact of the actual PTO system on the grid, future work will include laboratory HIL testing of the complete PTO hardware and grid connected to the real-time platform.

This work forms part of the project TAOIDE which is funded by the European Unions H2020 research and innovation programme under the grant agreement number 727465.

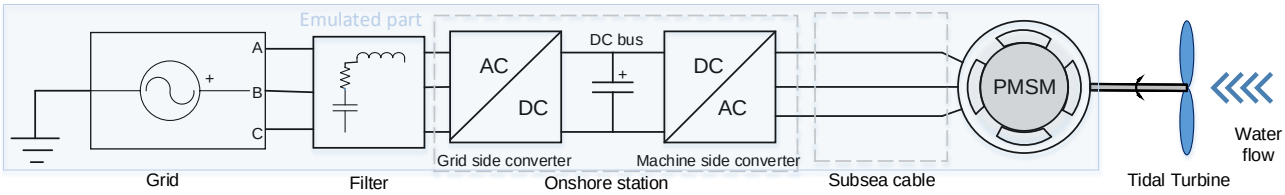

Fig. 1: Overview of the tidal energy test system studied.

II. Grid-connected Tidal Energy Test System

The schematic representation of the TES considered is illustrated in Fig 1. The complete PTO comprises a permanent-magnet synchronous machine (PMSM) rated 56 kW, 80 rpm, and about 7000 Nm, directly coupled to a tidal turbine (e.g., cross-flow turbine) and a bidirectional back-to-back converter and its controller. The turbine power curve is equal to zero during very low speeds. In this case, the PMSM is operated in motoring mode to accelerate the turbine, and once the turbine starts to develop torque on the machine shaft from interaction with the water flow, the direction of electrical power flow will change and power generation to the grid is maintained through the grid-side converter.

III. Modeling of the Complete Power Take-off System

A. Hydro-kinetic Cross-flow Turbine Model

The power at the shaft of the turbine provided by a water flow having a flow speed of v_{flow} passing the swept area A of the turbine is given by [13]

$$P_{turb} = \frac{1}{2} \cdot \rho \cdot A \cdot C_p \cdot v_{flow}^3, \tag{1}$$

The density ρ for sea water is 1025 kg/m^3 The power coefficient C_p depends on the operating condition and the design of the turbine. The operating condition is characterized by the tip speed ratio λ, which is defined as the ratio between speed at the tips of the turbine's blades and the flow speed:

$$\lambda = \frac{\omega_{turb} \cdot r_{turb}}{v_{flow}}, \tag{2}$$

where, ω_{turb} and r_{turb} are the rotational speed and radius of the turbine. The dependency of C_p on the tip speed ratio is obtained by computational fluid dynamics calculations shown in Fig 2.a. For measured water flow speed values in Fig 2.b, the mechanical power for a set rotational turbine speed (i.e., 55 rpm) is then obtained as shown in Fig 2.c.

B. Transmission Line Model

The turbine is typically placed close to shore with a relatively short one bundled cable run. Since the underground cable has large capacitance value, a nominal Pi model of the transmission line is used.

TABLE I: Machine Parameters Used.

R_s (Ω)	0.2781
R_g (Ω)	0.04
L_{ds}, L_{qs} (H)	0.0098
L_g (H)	0.001
P	16
λ_{fd} $(V \cdot s)$	3.9871
J $(kg \cdot m^2)$	225
T_f $(N \cdot m)$	238
B $(Nm \cdot s)$	4.017

C. Field-oriented PMSM Drive Model

The machine equations in the synchronously rotating reference frame are given by [14]

$$v_{ds} = R_s \cdot i_{ds} + L_{ds} \frac{d}{dt} i_{ds} - \omega_e \cdot L_{qs} \cdot i_{qs}, \tag{3}$$

$$v_{qs} = R_s \cdot i_{qs} + L_{qs} \frac{d}{dt} i_{qs} + \omega_e \cdot (L_{ds} \cdot i_{ds} + \lambda_{fd}), \tag{4}$$

$$T_e = \frac{3P}{2} \left(\lambda_{fd} \cdot i_{qs} + (L_{ds} - L_{qs}) i_{ds} \cdot i_{qs} \right) \tag{5}$$

$$T_{turb} = T_e + T_f + B \cdot \omega_m + J \frac{d\omega_m}{dt}, \tag{6}$$

where, $\omega_e = P\omega_m$. d and q denote the direct and quadrature axes quantities, v_s and i_s are stator voltage and current, R_s and L_s are stator winding resistance and inductance, respectively. λ_{fd} is rotor permanent magnet flux; P is the number of poles; ω_m is angular velocity of the turbine shaft; T_{turb} and T_e are turbine output torque and generated electromagnetic counter torque, respectively. T_f is static friction of the turbine. B and J are viscous friction and inertia of combined turbine and rotor shafts, respectively. The parameters of the model are listed in Table I.

The machine converter control employs a cascade control structure with inner and outer loops. The innermost torque controller is surrounded by the speed loop, which is in turn surrounded by the position loop. A field-oriented control scheme was developed utilizing cascaded speed and current control PI loops. A PI controller uses a speed error to create a reference q-axis current, which is directly proportional to machine torque. The controller to the PWM converter controls the machine terminal voltages to produce the d and q axis currents.

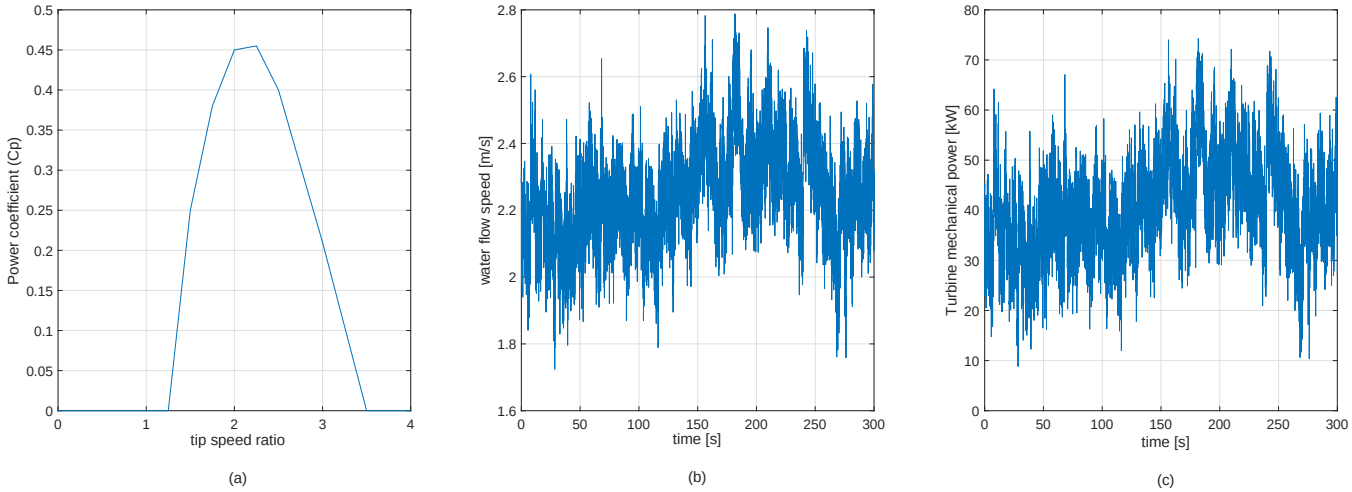

Fig. 2: a) Power coefficient of the turbine, b) measured water flow speed, c) emulated turbine output power.

D. Grid Side Converter Model

The grid side converter is assumed to be connected to a stiff grid through a series resistor R_g and inductor L_g. The voltage equations in the synchronously rotating reference frame are given by [15]

$$v_{dg} = R_g \cdot i_{dg} + L_g \frac{d}{dt} i_{dg} - \omega_g \cdot L_g \cdot i_{qg} + v_{dgrid}, \quad (7)$$

$$v_{qg} = R_g \cdot i_{qg} + L_g \frac{d}{dt} i_{qg} + \omega_g \cdot L_g \cdot i_{dg} + v_{qgrid}, \quad (8)$$

where, v_{dg} and v_{qg} are the per phase output voltages in quadrature axes from the converter while v_{dgrid} and v_{qgrid} are the corresponding voltages of the stiff grid. i_{dg} and i_{dg} are the currents flowing into the grid in quadrature axes. ω_g is the grid angular frequency.

The grid side converter is controlled to maintain the dc bus voltage at a desired level using PI controllers. Similar to the machine side converter control, the grid side converter control employs cascade voltage and current control loops with outer and inner loops for the active and reactive power, respectively. A PI controller uses a voltage error to thus create a reference d-axis current which is directly proportional to output active power, while the q-axis current can provide any desired reactive power requirements by setting a current reference to the second current controller. The active and reactive output powers can be expressed by [15]

$$P(t) = \frac{3}{2} i_{dg} \cdot v_{dgrid}, \quad (9)$$

$$Q(t) = \frac{3}{2} i_{qg} \cdot v_{dgrid}. \quad (10)$$

IV. Real-Time Emulation on a Parallel Hardware Platform

A. Real-Time Hardware Configuration

The hardware test rig is shown in Fig 3. It comprises a medium speed turbine emulator and a multicore CPU and FPGA-based hybrid real-time simulator. A re-configurable, 3 phase, 4 poles, 22 kW AC machine is used to emulate the turbine. The platform consists of one Intel processor core @3.0 GHz including a SPARTAN-3 FPGA card with 256 analog and digital I/O [16]. The complete PTO model has been tested in real-time on the platform while the characteristics of the tidal turbine for a given water flow condition are used as inputs to the simulator.

TABLE II: Real-time Simulation Parameters.

Major Computation time	5.17 μs
Acquisition (send to/recieved from the plant)	0.02 μs
Idle	3.14 μs
Time Step	10 μs
Switching frequency	8 kHz

To utilize the computational hardware resource efficiently, the model has been decoupled into four subsystems using the ARTEMiS-SSN solver [17]. The choice of a calculation time step is a compromise between simulation speed and resolution. The computational hardware needs 5.17 μs for execution of the model simulation and 0.02 μs for data sending to and receiving from the plant. To comply with the real-time behavior, a time step of 10 μs is therefore chosen. The real-time simulation parameters used are summarized in Table II. Considering the PWM switching frequency of 8 kHz used, the chosen time step is quiet sufficient to capture higher order dynamics. A real-time simulation is then performed. Special blocks on the target platform are used to acquire the values of variables for the first 3 seconds of the real-time simulation where a specific torque step change from 1 kNm to the rated value of 7 kNm occurs at 1 second. The dc bus is center tapped grounded with (+) and (-) 600 V either side. The voltages and currents at the machine and grid connection terminals including the dc bus voltage are observed.

B. Results and Discussion

Fig. 6 shows the PWM switching voltages and currents at the machine terminals. The open circuit voltage is 450 V (L-L)

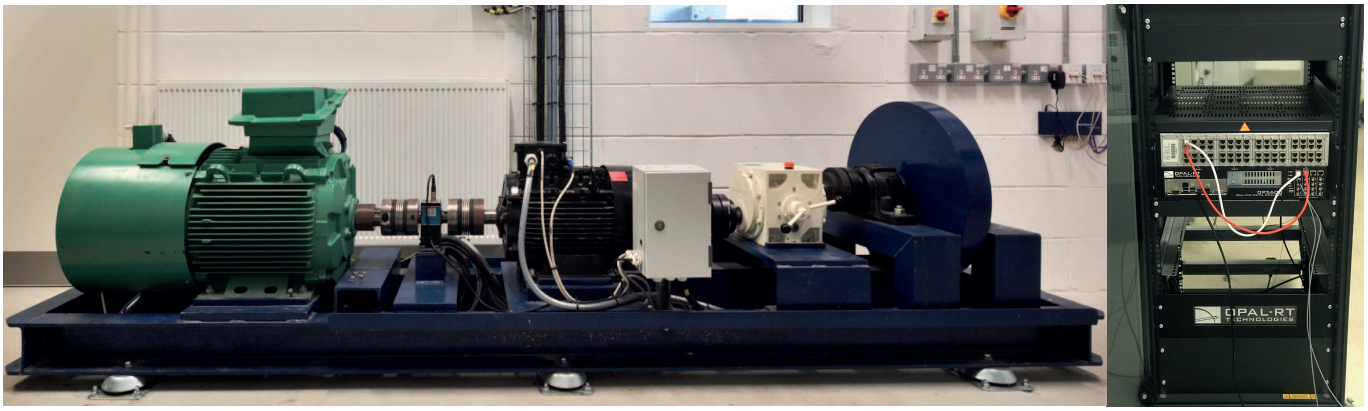

Fig. 3: Medium speed turbine emulator (left) and real-time simulator (right).

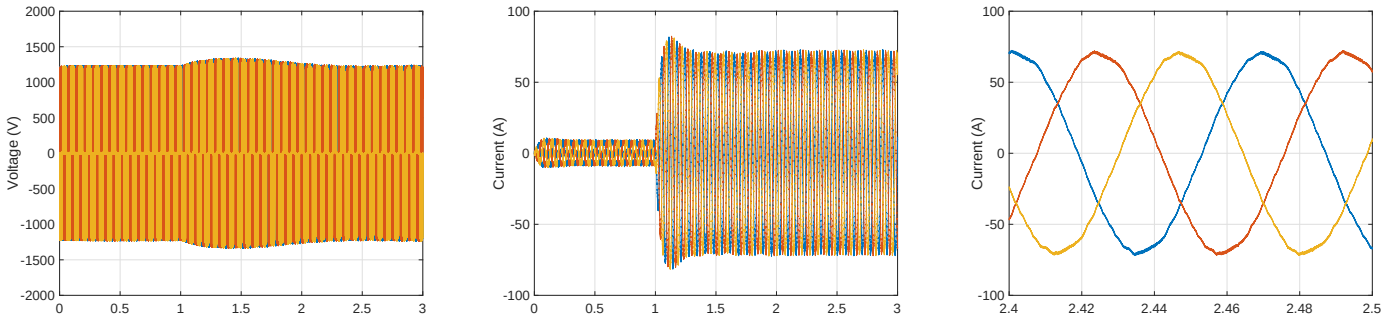

Fig. 4: Machine phase terminals: (a) voltages (b) currents (c) steady-state currents.

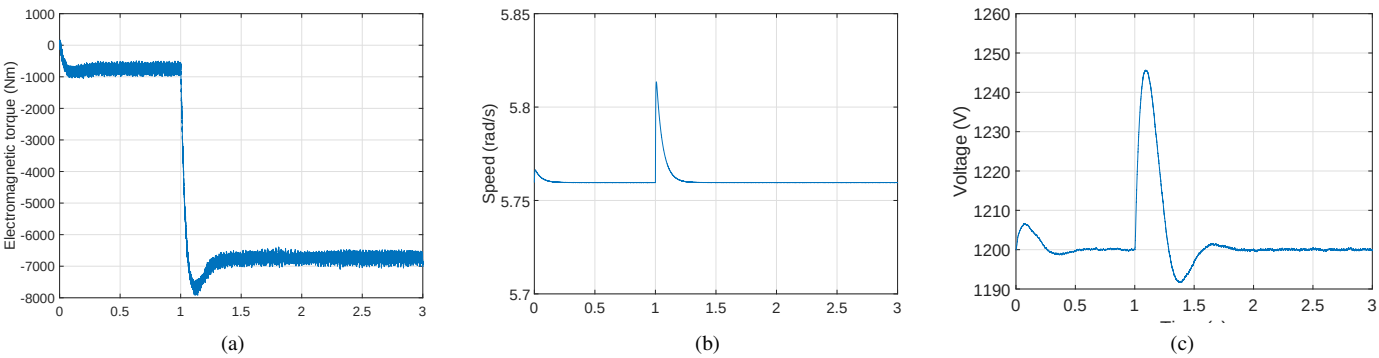

Fig. 5: (a) Electromagnetic counter-torque in the generator (b) generator speed (c) DC bus voltage.

which is equal to a peak phase voltage of 367.4 V. The average value in Fig. 4a is 367.8 V. The resulting electromagnetic torque is shown in Fig. 5a. Torque fluctuations are a result of the high frequency switching in the converter. To help maximize lifetime and reduce wear of mechanical components in the drive train, it is desirable to reduce the torque noise which will be investigated in the future. In response to a torque change from 1 kNm to 7 kNm at 1 s, the speed variation is given in Fig. 5b. As seen, the response of the speed controller is fast enough to settle the desired speed. For the step change in input torque, Fig. 5c demonstrates the dc bus voltage variation. The dc bus capacitor is seen to be a high stress component in the system. Filtering can be employed to alleviate that stress. To improve the power output through electrical storage options, supercapacitors connected to the dc bus have been investigated as an option for marine renewable technologies. Their demonstrated maintenance free long cycle life [18] can improve the power exported to the grid.

The currents and voltages at the common point of coupling are shown in Fig. 6a and 6b, respectively. To be able to quantify the quality of power being exported to the grid, THD of current signals is used as the voltage is ideal sinusoidal due to the stiff grid assumption. The switching frequencies up to 8 kHz do not violate the real-time behavior in our real-time setting. The THD values of the currents at steady-state for various switching frequencies are obtained as given in

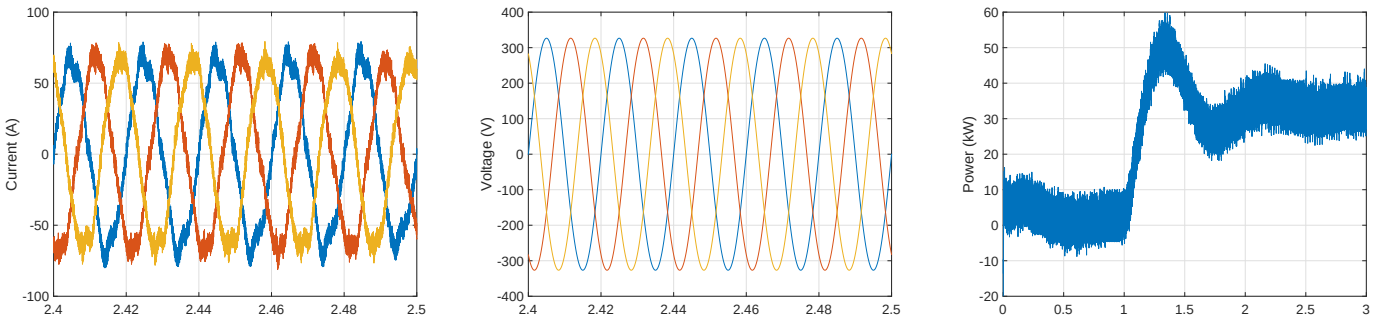

(a) (b) (c)

Fig. 6: (a) Grid currents (b) grid voltages (c) exported active power to the grid.

TABLE III: THD Measured of the Current.

Switching Frequency	THD
2 kHz	22%
4 kHz	12%
8 kHz	8%

Table III. As THD varies with the modulation index, it can be decreased for an increasing modulation index. Another option to help remove some of the noise from the grid side converter is to employ fine tuning of the filter. The grid voltages are seen to be an ideal stiff grid showing that irrespective of the active power exported shown in Fig.6c, the voltages stay the same. The mean value of reactive power is observed to be zero. To explore the system operation limits, the simulation is repeated for constant torque and constant power operations. The speed at maximum power is found to be 80 rpm while the maximum speed with field weakening is found to be 120 rpm.

V. Conclusion

The developed dynamic real-time simulation models proofed the system concept that incorporates a generator-frequency converter-system connected to the hydro-kinetic turbine to be valid. Operational limits and ratings were detailed through the real-time analysis. The developed model enables one to assess the power harvested by the hydro-kinetic turbine as well as the resulting power provided to the grid. Overall energy production and power quality can be evaluated.

Acknowledgment

This work forms part of the project TAOIDE which is funded by the European Unions H2020 research and innovation programme under the grant agreement number 727465.

References

[1] M. Santos, F. Salcedo, D.B. Haim, J.L. Mendia, P. Ricci, J.L. Villate, J. Khan, et al., “Integrating wave and tidal current power: Case studies through modelling and simulation,” IEA Implementing Agreement on Ocean Energy Systems (OESs), OES-IA No: T0331, pp. 178, 2011.

[2] J. Khan, G. Bhuyan, A. Moshref, ”Potential opportunities and differences associated with integration of ocean wave and marine current energy plants in comparison to wind energy,”, IEA Implementing Agreement on Ocean Energy Systems (OESs), Internainal Annex III Technical Report, OES-IA No: T0311, pp.64, 2009.

[3] M.C. Sousounis, J.K.H. Shek, and M.A. Mueller, “Modelling, control and frequency domain analysis of a tidal current conversion system with onshore converters,” IET Renewable Power Generation, vol. 10(2), pp. 158–165, 2016.

[4] D.O. Sullivan, J. Griffiths, James, M.G. Egan, and A.W. Lewis, ”Development of an electrical power take off system for a sea-test scaled offshore wave energy device,”Renewable Energy, Vol.36(4), pp.1236–1244, 2011.

[5] N. Erdogan, H. Henao, and R. Grisel, “A proposed Technique for Simulating the Complete Electric Drive Systems with a Complex Kinematics Chain,” in IEEE International Electric Machines Drives Conference (IEMDC), pp.1240–1245, 2007.

[6] J. G. Slootweg, S. W. H. de Haan, H. Polinder and W. L. Kling, ”General model for representing variable speed wind turbines in power system dynamics simulations,” IEEE Trans. Power Systems, Vol.18(1), pp.144–151, 2003.

[7] N. Erdogan, H. Henao, and R. Grisel, “The analysis of saturation effects on transient behavior of induction machine direct starting,” in IEEE Int. Symposium on Industrial Electronics, Vol.2, pp.975–979, 2004.

[8] A. Miller and E. Muljadi and D. S. Zinger, ”A variable speed wind turbine power control,” IEEE Trans. Energy Conversion, Vol.12(2), pp.181–186, 1997.

[9] N. Erdogan, T. Assaf, R. Grisel, and M. Aubourg, “An accurate 3-phase induction machine model including skin effect and saturations for transient studies,” in International Conference on Electrical Machines and Systems (ICEMS), Vol.2, pp.646–649, 2003.

[10] V. Jalili-Marandi, Z. Zhou, and V. Dinavahi, “Large-scale transient stability simulation of electrical power systems on parallel GPUs,” in IEEE Power and Energy Society General Meeting, pp.1–11, 2012.

[11] S. Mojlish, N. Erdogan, D. Levine, and A. Davoudi, “Review of hardware platforms for real-time simulation of electric machines,” IEEE Trans. Transportation Electrification, Vol.3(1), pp.130–146, 2017.

[12] G.G. Parma and V. Dinavahi, “Real-time digital hardware simulation of power electronics and drives,” IEEE Trans. Power Delivery, vol. 22(2), pp. 1235–1246, 2007.

[13] R. J. Cavagnaro, J. C. Neely, F. Fa, J. L. Mendia and J. A. Rea, ”Evaluation of Electromechanical Systems Dynamically Emulating a Candidate Hydrokinetic Turbine,” IEEE Trans. Sustainable Energy, Vol.7(1), pp. 390–399, 2016.

[14] A.A. Adam, K. Gulez, and N. Erdogan, “Minimum torque ripple algorithm with fuzzy logic controller for DTC of PMSM,” in International Conference on Intelligent Computing, pp.511–521, 2007.

[15] M. Chinchilla, S. Arnaltes and J. C. Burgos, ”Control of permanent-magnet generators applied to variable-speed wind-energy systems connected to the grid,” IEEE Trans. Energy Conversion, Vol.21(1), pp.130–135, 2006.

[16] Opal-RT Technologies, ”RT-LAB: distributed Real-Time platform ver. v11.2.2.108,”url = https://www.opal-rt.com/software-rt-lab/, 2017.

[17] C. Dufour, J. Mahseredjian, and J. Bélanger, ”A combined state-space nodal method for the simulation of power system transients,” IEEE Trans. Power Delivery, Vol.26(2), pp.928–935, 2011.

[18] D. B. Murray and J. G. Hayes, ”Cycle Testing of Supercapacitors for Long-Life Robust Applications,” IEEE Trans. Power Electronics, Vol.30(5), pp.2505–2516, 2015.